Surface & Coatings Technology 497 (2025) 131704

Contents lists available at ScienceDirect

Surface & Coatings Technology

journal homepage: www.elsevier.com/locate/surfcoat

Anti-corrosion and cytotoxicity properties of inorganic surface treatments on Mg1Ca biodegradable alloy

C.S. Neves [a,*], I. Sousa [a], M.A. Freitas [a], L. Moreira [b,c,d], C. Costa [b,c,d], J.P. Teixeira [b,c,d], S. Fraga [b,c,d,e], R.M. Silva [a], R.F. Silva [a], M. Starykevich [a], N. Scharnagl [f], M.L. Zheludkevich [f,g], M.G.S. Ferreira [a], J. Tedim [a]

[a] Department of Ceramics and Materials Engineering, CICECO, University of Aveiro, 3810-193 Aveiro, Portugal
[b] Department of Environmental Health, National Institute of Health Dr. Ricardo Jorge, Rua Alexandre Herculano 321, 4000-055 Porto, Portugal
[c] EPIUnit-Institute of Public Health, University of Porto, Rua das Taipas 135, 4050-600 Porto, Portugal
[d] Laboratory for Integrative and Translational Research in Population Health (ITR), Rua das Taipas 135, 4050-600 Porto, Portugal
[e] Department of Biomedicine, Unit of Pharmacology and Therapeutics, Faculty of Medicine, University of Porto, Alameda Prof. Hernani Monteiro, 4200 - 319 Porto, Portugal
[f] Institute of Surface Science, Helmholtz-Zentrum Hereon, Max-Planck Straße 1, 21502 Geesthacht, Germany
[g] Institute for Materials Science, Faculty of Engineering, University of Kiel, Kaiserstraße 2, 24143 Kiel, Germany

ARTICLE INFO

Keywords:
Mg1Ca alloy
Inorganic surface treatments
In vitro cytotoxicity
Corrosion

ABSTRACT

In this work biodegradable Mg1Ca alloy underwent surface modification using hydroxyapatite (HAp), aluminium oxide (Al_2O_3), and treatments with phosphoric (H_3PO_4), hydrofluoric (HF), and acetic (CH_3COOH) acids. The resulting surface-treated Mg substrates were assessed in terms of phase content and chemical composition through X-ray diffraction (XRD) and glow discharge optical emission spectrometry (GDOES). Additionally, atomic force microscopy (AFM) and scanning electron microscopy (SEM) were employed to examine the surface's topography and structure, while the corrosion behavior and cytotoxicity were surveyed using electrochemical impedance spectroscopy (EIS), alongside WST-1 reduction and lactate dehydrogenase (LDH) release assays on L929 mouse fibroblasts. The findings indicated that the surfaces of all samples were uniformly structured, while chemical analysis of the treated surfaces suggested the presence of mostly thin films. Furthermore, EIS results highlighted that the HAp-treated Mg1Ca alloy exhibited superior corrosion resistance, and the cytotoxicity assessment of Mg1Ca-HAp and Mg1Ca-H_3PO_4 alloys showed minimal cytotoxic effects on mouse fibroblasts, compared to other treated surfaces, suggesting enhanced biocompatibility of those two surface treatments. Overall, this constitutes the first comparative study of different surface treatments developed on biodegradable Mg1Ca alloy, aiming to identify optimal modification strategies for biomedical applications.

1. Introduction

Magnesium (Mg) alloys are recognized for their mechanical strength, biocompatibility, and rapid dissolution, qualities that render them ideal for use in biomedical fields [1]. However, the practical deployment of Mg alloys as biodegradable materials faces obstacles due to their uncontrolled reactive nature and a tendency toward corrosion, which often leads to hydrogen production and localized alkalization [2,3]. Ironically, what is considered one of Mg alloys' key benefits – their fast dissolution – also presents a significant challenge. To mitigate these issues, a range of tactics has been employed. These include developing new Mg alloy compositions through the introduction of alloying elements [4,5], as well as employing surface treatments [5,6] designed to reduce corrosion rates to manageable levels of degradation [7].

Incorporating elements like aluminium (Al), Rare Earth Elements (REE), zinc (Zn), and calcium (Ca) into Mg alloys can markedly enhance their mechanical strength, resistance to corrosion, and biocompatibility [8]. Nevertheless, it is crucial to closely monitor the alloying elements due to the possible toxicity risks they present. This is particularly important because the significant release of Mg and other potentially hazardous elements during biodegradation can result in elevated cytotoxicity levels [9]. In contrast to pure Mg, incorporating Al as an alloying

* Corresponding author.
E-mail address: cristina.neves@ua.pt (C.S. Neves).

https://doi.org/10.1016/j.surfcoat.2024.131704
Received 17 October 2024; Received in revised form 13 December 2024; Accepted 23 December 2024
Available online 26 December 2024

element enhances both the mechanical strength and corrosion resistance [10]. However, it is important to note that Al is a recognized neurotoxicant which, in high concentrations, can damage the nervous system and may be linked to various neurological disorders [3,9,11]. Consequently, the release of Al from Mg alloys needs to be strictly regulated to avoid Al-induced neurotoxicity. On the other hand, REE are usually added to Mg alloys to increase their mechanical strength and corrosion resistance [12]. To this end, several Mg alloys containing REE, including WE43, Mg5Gd, and LAE442, have been explored [13]. Yet, similar to the use of Al, a careful balance between potential toxicity and benefits must be maintained. This is because the inclusion of elements like cerium (Ce), praseodymium (Pr), and yttrium (Y) is linked with severe liver toxicity [14]. Therefore, beyond certain concentrations, Al and REE are considered inappropriate as alloying elements in biomedical Mg materials.

In this quest for novel biodegradable Mg alloys without Al, REE or other harmful elements, some studies have reported Zn and Ca as appropriate alloying elements for Mg [15–18]. Zn and Ca are both biological and essential elements in the human body. Due to these characteristics, Mg alloys containing Zn and/or Ca such as Mg1Zn, Mg1Ca or Mg5Ca have been proposed, in the past years, for the development of biodegradable implants [9,19,20]. Zn is used to improve the strength and lower the corrosive effect of iron (Fe) and nickel (Ni) impurities [21], while Ca is used to improve corrosion resistance and thermal stability of Mg [19,22]. Moreover, Ca also improves the biocompatibility of the alloys [4]. In a recent study of our research group [3] we have compared Mg1Ca with the biodegradable Mg10Gd alloy in terms of corrosion rate and induced cytotoxicity. Our findings showed that Mg1Ca exhibits a slower degradation rate compared to Mg10Gd. This reduced degradation is attributed to the incorporation of Ca as an alloying element, which enhances the stability of the corrosion product layer formed in various electrolytes. Furthermore, in cytotoxicity assessments, Mg10Gd displayed toxicity under all tested conditions, whereas Mg1Ca demonstrated minimal toxicity.

Although Mg1Ca alloy exhibits improved corrosion resistance and favorable biological characteristics, the sole use of alloying falls short in achieving the necessary level of corrosion resistance. This shortfall is due to the negative potential of Mg ($E^\circ = -2.4$ V vs. SHE), anomalous HE in water [23] and its weak tendency to form passive layers. Additionally, localized forms of corrosion like pitting corrosion, often resulting from inhomogeneous microstructures in Mg alloys, may accelerate the corrosion processes [3]. Therefore, taking into consideration the bio-based applications of this alloy, it is critical to minimize the localized corrosion to maintain its mechanical strength and reduce pernicious side effects, such as hydrogen evolution, that may occur during the alloy service time. This can be achieved through the application of surface treatments able to form a protective layer, which can delay the direct contact between Mg alloys and the surrounding environment allowing to control the fast degradation of the alloys [24]. These surface treatments can include chemical, physical and mechanical treatments as well as surface modification with coatings.

Regarding MgCa biodegradable alloys, different surface modification methods have been reported namely, conversion coatings resulting from acid pickling [25,26], calcium phosphate [27] (CaP) and magnesium fluoride [28] (MgF_2) coatings, microarc oxidation [29], surface modification with polymer coatings [30–33] and mechanical surface treatment such as laser shock peening (LSP) [34] and burnishing [35]. These methods have shown to decrease the corrosion rate of the alloys while improving biomineralization [25,26,28,32,33] and enhancing cell affinity [27,28,31]. Despite these advancements, surface modification methods still present significant limitations, including difficulties in producing defect-free coatings (e.g., pores), poor adhesion, and the inherent tendency of Mg alloys toward localized corrosion [36,37]. Additionally, the corrosion products of Mg alloys are not impermeable, which further compromises their protective capabilities even after surface treatments [36,37].

Most corrosion evaluation and biocompatibility tests reported so far, have been performed under simplified physiological environments, such as simulated body fluid - SBF or Hanks' solution. However, bearing in mind the bioapplications of the alloys, a more complex and representative environment should be considered. Minimum Essential Media (MEM), a widely used cell culture medium, is not only significant for in vitro cell growth and toxicity assays but also offers active corrosion protection to MgCa alloys, as previously reported by our group [3]. Additionally, MEM effectively replicates an in vivo setting, closely resembling the protein composition of mammalian cells [38]. While its Ca and Mg content is marginally lower than that found in blood, MEM contains glucose, a higher concentration of amino acids, vitamins, and comparable concentrations of HPO_4^{2-} and HCO_3^-, making it a more reliable medium to mimic in vivo behavior of different materials.

In this study, we present a compreenshive investigation of the impact of five distinct surface treatments on the surface morphology, electrochemical corrosion properties, and cytotoxicity of the biodegradable Mg1Ca alloy, using MEM as the selected immersion medium. Our study systematically compares a range of surface treatments, including conversion layers obtained via acid pickling with phosphoric (H_3PO_4), hydrofluoric (HF), and acetic (CH_3COOH) acids, chemical surface modification with hydroxyapatite (HAp), and growth of aluminium oxide (Al_2O_3) by atomic layer deposition (ALD). This comparative analysis provides a detailed examination of their effects on corrosion resistance and cytotoxicity, which has not been extensively covered in existing literature. Conversion coatings were applied due to their simplicity and low cost. Acid pickling, in particular, promotes the formation of thin films on the substrate surface, constituting a protective layer that can delay the subsequent corrosion of the Mg1Ca alloy [8]. Chemical surface treatment provides initial protection from corrosion, with inorganic coatings such as HAp improving the biocompatibility of the substrate [39]. On the other hand, ALD is an innovative technique for depositing of thin films with precise thickness control, offering a promising way to overcome the corrosion susceptibility of Mg alloys. Therefore, the present study aims to identify a surface treatment that not only reduces Mg1Ca degradation from corrosion but also improves its surface cytocompatibility.

The novalty of our work lies in three key aspects: (i) Multi-technique approach where a robust combination of analytical techniques was employed including GDOES, SEM-EDS, AFM, XRD, EIS and SEM cross-sectional analysis. This multi-faceted approach provides a thorough and reliable investigation of the coatings, enhancing the depth and accuracy of our findings. This synergy between techniques allows for a deeper understanding of coating performance than any single method could provide; (ii) Comprehensive comparison, providing a unique comparative analysis of different surface treatments, assessing their impact on corrosion resistance and cytotoxicity in a single framework; (iii) Use of Minimum Essential Media (MEM), which was used as a more reliable medium for evaluating the real-world biomedical performance of the materials, in contrast to many studies that utilize simpler physiological environments such as SBF or Hanks' solution. This distinction further highlights the innovation and practical relevance of our research.

Overall, our study aims fill a critical knowledge gap by identifying and validating surface treatments that reduce Mg1Ca degradation while enhancing cytocompatibility. The insights gained from this research are expected to contribute to the development of more effective surface treatments for Mg alloys, with potential applications in biomedical field.

2. Experimental section

2.1. Materials

2.1.1. Chemicals

All the chemicals used in this study were bought from Sigma-Aldrich at an analytical grade and used in its original form without additional

purification. The cell culture medium, supplements, and reagents were acquired from Gibco, Thermo Fisher Scientific, USA.

2.1.2. Metal substrates

The biodegradable Mg alloy Mg1Ca chosen for the proposed research, was cast at the Helmholtz-Zentrum Hereon in Geesthacht, Germany. The chemical composition of this alloy was previously reported [3].

2.1.3. Surface treatment of Mg alloys

Before surface treatment, the metal substrate surfaces were polished using silicon carbide (SiC) paper (from 400 to 2500 grit), rinsed with isopropanol and dried in a warm stream of air.

For the surface treatment of Mg1Ca substrates five protocols were defined (see Fig. 1), which included acid pickling with phosphoric acid (H_3PO_4) (Treatment 1), hydrofluoric acid (HF) (Treatment 2) and acetic acid (CH_3COOH) (Treatment 3), an aluminium oxide (Al_2O_3) layer obtained by ALD (Treatment 4) and a hydroxyapatite ($Ca_5(PO_4)_3(OH)$) layer obtained by hydrothermal treatment (Treatment 5).

In Treatment 1 substrates were immersed in a 40 g/L phosphoric acid solution for 60 s, following a procedure from literature [40], while for Treatments 2 and 3 the substrates were immersed, respectively, in a 140 g/L hydrofluoric [41] acid solution for 60 min [41] and a 300 g/L acetic acid solution for 120 min [42]. All the samples were then rinsed with deionized water and dried with a warm stream of air.

The deposition of Al_2O_3 (Treatment 4) was performed using a homemade cross-flow ALD reactor working in exposure mode at 200 °C, as described elsewhere [43]. To this end, trimethylaluminum ($C_6H_{18}Al_2$) was used as the Al source and was kept in a stainless steel reservoir at room temperature. The other precursor, water (H_2O) was kept in the stainless steel reservoir also at room temperature. The reactor body was continuously purged with 100 sccm of dry N_2 for a baseline reactor pressure of 2.1 Torr. The delivery lines were maintained at 100 °C to minimize precursor condensation throughout the depositions. To ensure saturation behavior, the pulse time for both precursors was set accordingly. In a typical ALD cycle, the first precursor was pulsed for 0.5 s, and the second precursor was pulsed for 1.0 s. Subsequently, both precursors were held in the deposition chamber for 20 s before a 30-s pump step. Several samples with 400 ALD cycles were prepared.

Regarding Treatment 5, a procedure available in the literature was followed [44], in which Mg1Ca substrates were immersed in a mixture of 250 mM of ethylenediaminetetraacetic acid calcium disodium salt hydrate (Ca-EDTA: $C_{10}H_{12}N_2O_8Na_2Ca$) solution with a 250 mM of potassium dihydrogen phosphate (KH_2PO_4) solution for 6 h at 90 °C. The pH of the mixture was adjusted to 8.9 using sodium hydroxide (NaOH).

The labels of the surface-treated substrates are as follows: Mg1Ca-H_3PO_4 (Treatment 1); Mg1Ca-HF (Treatment 2); Mg1Ca-CH_3COOH (Treatment 3); Mg1Ca-Al_2O_3 (Treatment 4) and Mg1Ca-HAp (Treatment 5).

2.2. Methods

2.2.1. Morphology and crystal structure characterization

The topographical features of the samples were analyzed using a Hitachi S-4100 scanning electron microscope, with incorporated energy dispersive spectroscopy (SEM-EDS). This system was operated at an acceleration voltage of 25 kV for detailed morphological characterization.

The crystal structure and phase composition of the samples were determined through X-Ray Diffraction (XRD) analysis. This was conducted at ambient temperature with a PANalytical X'Pert MPD PRO diffractometer, employing Bragg-Brentano geometry and Ni-filtered Cu Ka radiation with a PIXcel1D detector. The measurements were taken in steps of 0.02°, with an exposure time of approximately 2 s per step, across an angular range from 4 to 80°.

2.2.2. Topography analysis

Atomic Force Microscopy (AFM) was used to assess the roughness of the samples. The procedure involved using a multimode atomic force microscope, specifically the Nanoscope IV model, originally produced by Veeco Instruments and now part of Bruker Corporation. The imaging process was conducted in tapping mode, employing silicon probes that resonate at approximately 320 kHz with a force constant of 42 N/m. The analysis of these images was carried out using the Gwyddion software, version 2.37. The Root Mean Square (RMS) roughness values, denoted as Rq, were extracted directly from the surface topography images with the aid of Gwyddion software. This software calculates Rq using the following formula:

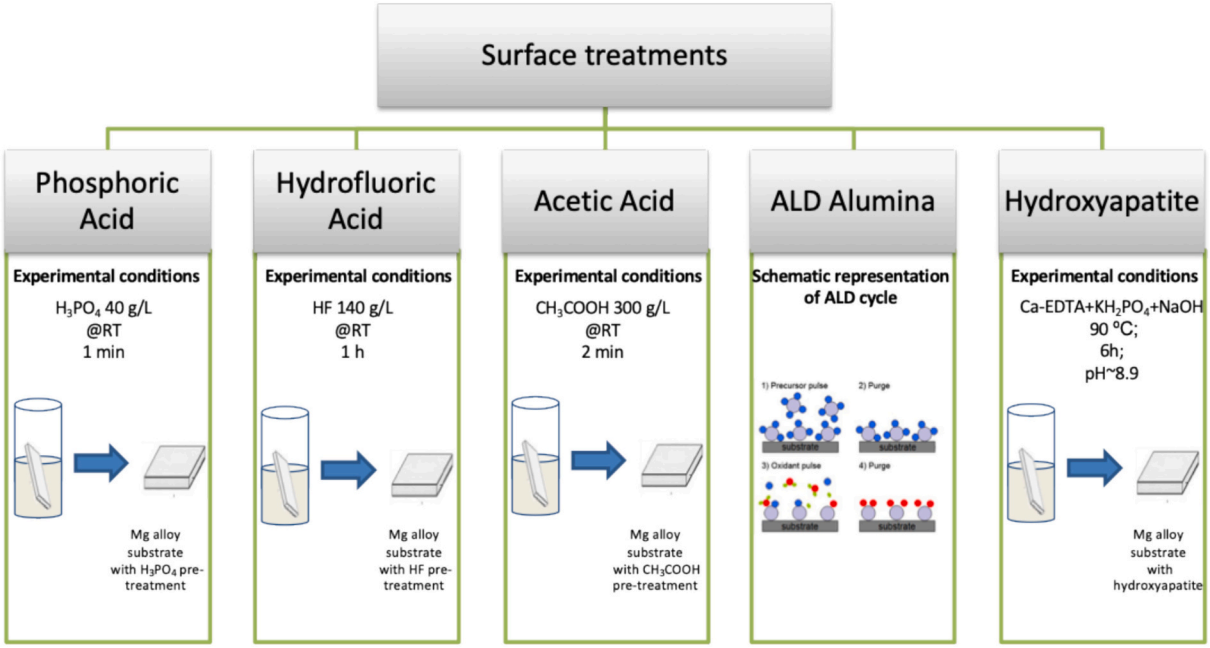

Fig. 1. Schematic representation of the different surface treatments applied to Mg1Ca surface.

$$Rq = \sqrt{\frac{1}{L}\int_0^L Y^2(X)dx}$$

In this equation, L represents the length of the profile measured along the x-axis, and Y(X) denotes the height variation from the profile line at each data point.

2.2.3. Chemical analysis of surface treatments

Comprehensive chemical analysis and surface profiles assessments of the applied surface treatments were executed using glow discharge optical emission spectrometry (GDOES). The depth profiling analysis employed a HORIBA GD-Profiler 2, integrated with a copper anode of 4 mm diameter. This methodology involved the implementation of argon sputtering on the specimen surface, regulated at a pressure of 650 Pa and an operational power of 30 W.

2.2.4. Electrochemical studies

The corrosion behavior of Mg1Ca substrates was examined through the application of electrochemical impedance spectroscopy (EIS). For EIS experiments, a tri-electrode configuration was used, comprising a SCE reference electrode, a platinum foil as the counter electrode, and the Mg alloy (Mg1Ca) serving as the working electrode with an exposed area of approximately 2.27 cm^2. To mitigate the effects of external electromagnetic disturbances, the entire setup was enclosed within a Faraday cage. Given its significance in biological contexts, MEM was chosen as the electrolyte (referenced in Table 1) [3]. The EIS data acquisition was performed using a Gamry interface 1000 potentiostat. The selected frequency range for these tests was from 10^5 to 10^{-2} Hz, applying a sinusoidal perturbation of 10 mV rms across 10 points per frequency decade. These spectra were all recorded at open circuit potential, under standard atmospheric conditions and room temperature. To ensure consistency, each measurement was conducted in triplicate, verifying the reproducibility of the findings.

2.2.5. Preparation of Mg1Ca alloy extracts for cytotoxicity testing

Mg1Ca alloy extracts were prepared as previously described [3], and according to ISO 10993-12:2021 [45]. Briefly, the alloys were cut into circular disks with a diameter of 1.7 cm, thickness of 0.5 cm, sterilized by UV radiation for 2 h (1 h per disk side), and incubated for 24 h and 72 h at 37 °C in borosilicate glass containers with MEM containing 4 mM L-glutamine, 100 units/mL of penicillin and 100 μg/mL of streptomycin, at a surface area-to-extractant volume ratio of 1.25 cm^2/mL. For preventing sorption onto the extraction container or other changes in their composition, the liquid extracts were tested for cytotoxicity immediately after the end of the incubation period.

2.2.6. In vitro cytotoxicity testing of the Mg1Ca alloy extracts in L929 mouse fibroblasts

The cytotoxicity of the Mg1Ca alloy extracts was tested in mouse fibroblast L929 cells, according to ISO 10993-5:2009 [46]. L929 cells (American Type of Culture Collection; CCL1) were cultured in MEM supplemented with 4 mM L-glutamine, 100 units/mL of penicillin, 100 μg/mL of streptomycin and 10 % of heat inactivated fetal bovine serum (FBS), in a humidified atmosphere of 5 % CO_2–95 % air at 37 °C. Cells were subcultured at 80 % confluence with trypsin-EDTA 0.25 % solution and seeded in flat bottom 96-well plates (10.000 cells/well). The medium was changed 24 h after seeding. At 48 h after seeding, cells were exposed for 24 h to the as extracted (1×), as well as to 1:2, 1:4 and 1:8 extract's dilutions. Control cells were exposed to the extraction medium diluted in the same % of the tested extracts. Cytotoxicity was investigated in the same cells simultaneously by the WST-1 reduction and lactate dehydrogenase (LDH) release assays. Cells incubated for 30 min with 70 % ethanol served as positive controls (PC) for the WST-1 reduction assay, while for the LDH release assay PC cells were incubated with 0.2 % Triton X-100. For LDH release determination, the incubation medium of each well was collected and centrifuged for 5 min at 2000 x*g* to remove the cell debris before analysis. The assay was carried out according to the manufacturer's instructions (Roche Applied Sciences, Mannheim, Germany). Absorbance was measured in a microplate reader (SpectraMax iD3, Molecular Devices, USA) at 490 nm and 630 nm (reference wavelength). Data was expressed in percentage of LDH release relative to the PC (total LDH release).

For WST-1 reduction quantification, cells incubated for 2 h at 37 °C and 5 % CO_2 with 100 μL/well of Cell Proliferation Reagent WST-1 (Roche Applied Sciences, Mannheim, Germany) diluted 1:10 in FBS-free cell culture medium. Absorbance was measured at 450 nm and 630 nm (reference wavelength). Data was expressed in percentage of the negative control (NC) response.

Table 1
Composition of the selected electrolyte.

MEM (Minimum essential medium)	
$CaCl_2.2H_2O$	0.26 g/L
$MgSO_4.7H_2O$	0.20 g/L
NaCl	6.8 g/L
KCl	0.40 g/L
$NaHCO_3$	2.2 g/L
$NaH_2PO_4.2H_2O$	0.16 g/L
Amino acids	
Vitamins	
D-Glucose	
Phenol Red	

3. Results and discussion

3.1. Surface morphology characterization

In Fig. 2 is possible to observe the visual aspect of the untreated Mg1Ca alloy, as well as the substrates subjected to the five surface treatments. The untreated surface presents some scribes that arise from the polishing step done before the surface treatment step. These scribes are not observed in the treated samples, indicating that changes in the substrates surface have occurred, due to the formation of conversion films or deposition of inorganic layers. After the surface treatment, all samples presented a regular uniform appearance, although with different morphologies. These observations are in accordance with the results obtained by SEM and AFM, presented in Fig. 3.

SEM image of the untreated Mg1Ca alloy (Fig. 3-A1) presents the original grinding grooves from the polishing procedure while EDS spectrum (Fig. 3-A2) shows that the alloy is mainly constituted by Mg with a small amount of Ca. Taking into account the treatments based on acid pickling (as shown in Fig. 3 B, C and D), the surface morphology varies depending on the specific acid used and the duration of treatment. For the Mg1Ca-H_3PO_4 sample, the interaction of phosphoric acid with the alloy's surface led to the formation of a conversion coating, characterized by a distribution of cracks throughout the surface (Fig. 3-B1). The EDS spectrum presented in Fig. 3-B2 for Mg1Ca-H_3PO_4 is similar to that of the bare substrate (Fig. 3-A2), having only two small additional peaks associated with the presence of P and O, which can be associated with the formation of a phosphate-containing film on the surface [26]. Since the intensity of Mg peak is higher than that of P and O, the formed film is possibly thin. In the case of Mg1Ca-CH_3COOH sample, the SEM image (Fig. 3-C1) shows that the acid etching led to removal of surface material, with formation of a thin film with pores spread around the whole surface. Furthermore, EDS spectrum shows the presence of small peaks of C and O that can be related with the formation of a magnesium acetate film (Fig. 3-C2) [25]. The Mg substrate treated with hydrofluoric acid (Mg1Ca-HF, Fig. 3-D1) shows a distinct grooved surface morphology characterized by regularly spaced and well-defined linear features, covering the entire treated surface area. The presence of fluoride in EDS spectrum (Fig. 3-D2) indicates that HF was involved in the formation of a surface layer with possible formation of $Mg(OH)_xF_{2-x}$

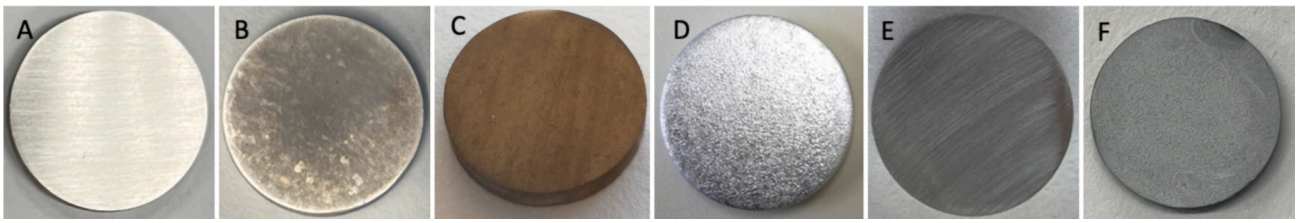

Fig. 2. Photographs of (A) untreated Mg1Ca alloy and (B) Mg1Ca-H_3PO_4; (C) Mg1Ca-HF; (D) Mg1Ca-CH_3COOH; (E) Mg1Ca-Al_2O_3 and (F) Mg1Ca-HAp treated substrates.

compounds [47] or MgF_2 conversion films [48,49]. This surface layer is suggested to be very thin, as evidenced by the small intensities of F and O peaks compared to Mg.

Regarding to the deposition of Al_2O_3 film onto Mg1Ca surface (Mg1Ca-Al_2O_3, Fig. 3-E1) the deposited layer presents grooves and striations. This morphology can be associated with the scribes that the substrate presented before the ALD step (Fig. 3-A1), since ALD is a technique in which the deposited films are conformal with the substrate surface [50,51]. Moreover, the EDS spectrum (Fig. 3-E2) supports the thin film assumption, since the intensity of the element peaks Al and O are very small when compared to the Mg signal. The surface morphology of Mg1Ca-HAp treated sample obtained by SEM is shown in Fig. 3-F1. The morphological features reveal a regular flake-like structure, uniformly covering the substrate surface. The elemental composition of the Mg1Ca-HAp obtained by EDS (Fig. 3-F2), reveals the presence of O, P and Ca indicating the formation of a layer containing calcium phosphate ($Ca_3(PO_4)_2$), that may correspond to hydroxyapatite ($Ca_{10}(PO_4)_6(OH)_2$) [52,53]. It can also be observed that the intensity of Ca and P peaks is higher compared to Mg, suggesting that the film formed on the substrate surface is thicker compared to those discussed previously.

After considering the EDS spectra, it is important to note that due to the thin nature of the investigated conversion layers, except for HAp, the electron beam used in imaging penetrates through most of the layer. As a result, the EDS spectra primarily capture the composition of the underlying Mg substrate. This occurrence is directly linked to the utilization of a high acceleration voltage, which affects a depth well beyond 10 μm. To put it simply, the low signal observed in the EDS spectra for the elements constituting the conversion layers, is a direct outcome of this high acceleration voltage phenomenon over the minimal thickness of the samples.

The surface morphology was also analyzed by AFM and the topographic images obtained for all the surface treatments are depicted in Fig. 3-A3 to Fig. 3-F3. The surface morphology revealed by AFM matches that obtained by SEM. However, some surface features can be observed with more detail. In the case of the bare substrate the polishing step renders a texture of striations that is easily seen in the AFM image (Fig. 3-A3). Mg1Ca-H_3PO_4 sample presents a surface morphology with step bunching (Fig. 3-B3), indicating the presence of a film structure with various heights that are related with the cracks formed after film drying. AFM surface topography image of Mg1Ca-CH_3COOH presents a smooth surface with no pronounced grains (Fig. 3-C3), while Mg1Ca-HF shows grooves with consistent depth and width (Fig. 3-D3), indicating a controlled and uniform etching process during the hydrofluoric acid treatment. The AFM image of ALD-treated substrate (Fig. 3-E3) is quite similar to that of the bare substrate (Fig. 3-A3), meaning that the deposited film is thin, and conformal with the substrate surface, so the main edges and grooves resulting from the polishing step of the bare substrate remain noticeable. Mg1Ca-HAp presents various fine structures randomly laid on the sample surface (Fig. 3-F3), indicating the formation and deposition of a nanostructured film uniformly covering the substrate surface.

From the AFM images it was also possible to extract the root mean square (RMS) roughness of the treated surfaces, and the obtained values are shown in Table 2. There is a difference in the roughness values from the bare substrate to the pre-treated samples and with the exception of Mg1Ca-CH_3COOH and Mg1Ca-Al_2O_3, the RMS roughness values increase after the surface treatment. The surface treated with H_3PO_4 (Mg1Ca-H_3PO_4), shows the highest roughness value, followed by Mg1Ca-HAp and Mg1Ca-HF (736 nm, 409 nm and 253 nm, respectively). The higher roughness of the Mg1Ca-H_3PO_4 sample is attributed to the extensive cracked film on its surface, resulting in larger differences between peaks and valleys. This trend is also observed in the case of Mg1Ca-HAp sample, where the deposition of a layer composed of flake-like structures with different sizes, shapes and orientations, can contribute to the larger roughness of this sample compared to the substrate without treatment. Regarding the Mg1Ca-HF sample, the hydrofluoric acid etching resulted in a slight surface roughning compared to the bare substrate. Considering the surface roughness of the Mg1Ca-Al_2O_3, this is similar to that of the bare substrate, indicating the deposition of a thin layer of Al_2O_3 with high conformality, thereby not significantly changing the substrate roughness. On the other hand, CH_3COOH etching (Mg1Ca-CH_3COOH) led to the smoothest surface finishing. In this case, the etching allowed to remove unevennesses from processing, such as the grinding marks, as well as to uniformly remove impurities from the surface, which render the surface with a lower roughness.

Overall, the results obtained by SEM and AFM demonstrate that the type of surface treatment influences the surface topography as well as roughness properties.

3.2. Phase composition and crystal structure

The XRD patterns acquired from the pre-treated samples are shown in Fig. 4. As it can be seen from the patterns of the different surface treatments (Fig. 4 A) only the substrate peaks (marked as Mg) are mainly observed, as demonstrated by the peaks at 2θ angles around 32°, 34°, 36°, 47°, 57° and 63° corresponding to (100), (002), (101), (102), (110) and (103) crystal planes of Mg respectively (JCPDS card number 04–003-5290).

However, in the case of hydroxyapatite and phosphoric acid surface treatments, additional peaks can be observed (Fig. 4 B), which corresponds to HAp and $Ca_3(PO_4)_2$ phases. Mg1Ca-HAp present peaks at 2θ angles around 26°, 28°, 29°, 49°, 51° and 53° corresponding to (002), (102), (210), (213), (312) and (004) crystal planes indexed to $Ca_{10}(PO_4)_6(OH)_2$ (JCPDS card number 00–064-0738). In the case of Mg1Ca treated with phosphoric acid (Mg1Ca-H_3PO_4), the diffractogram presents peaks at 2θ angles around 23°, 26°, 27° and 29° related with (132), (043), (−334) and (004) crystal planes of $Ca_3(PO_4)_2$, respectively (JCPDS card number 00–029-0359).

In the particular case of Mg1Ca-Al_2O_3 sample, no peaks corresponding to Al_3O_3 film are detected, which is consistent with the literature reporting that Al_2O_3 films deposited below 400 °C tend to form an amorphous structure [54]. This absence of peaks from the coating further supports the amorphous nature of the deposited film.

For the Mg1Ca-HF and Mg1Ca-CH_3COOH treatments, the XRD patterns primarily show peaks attributed to the Mg substrate, suggesting that the films formed are essentially amorphous. The short durations of the chemical treatments (60 min for HF and 2 min for CH_3COOH) likely

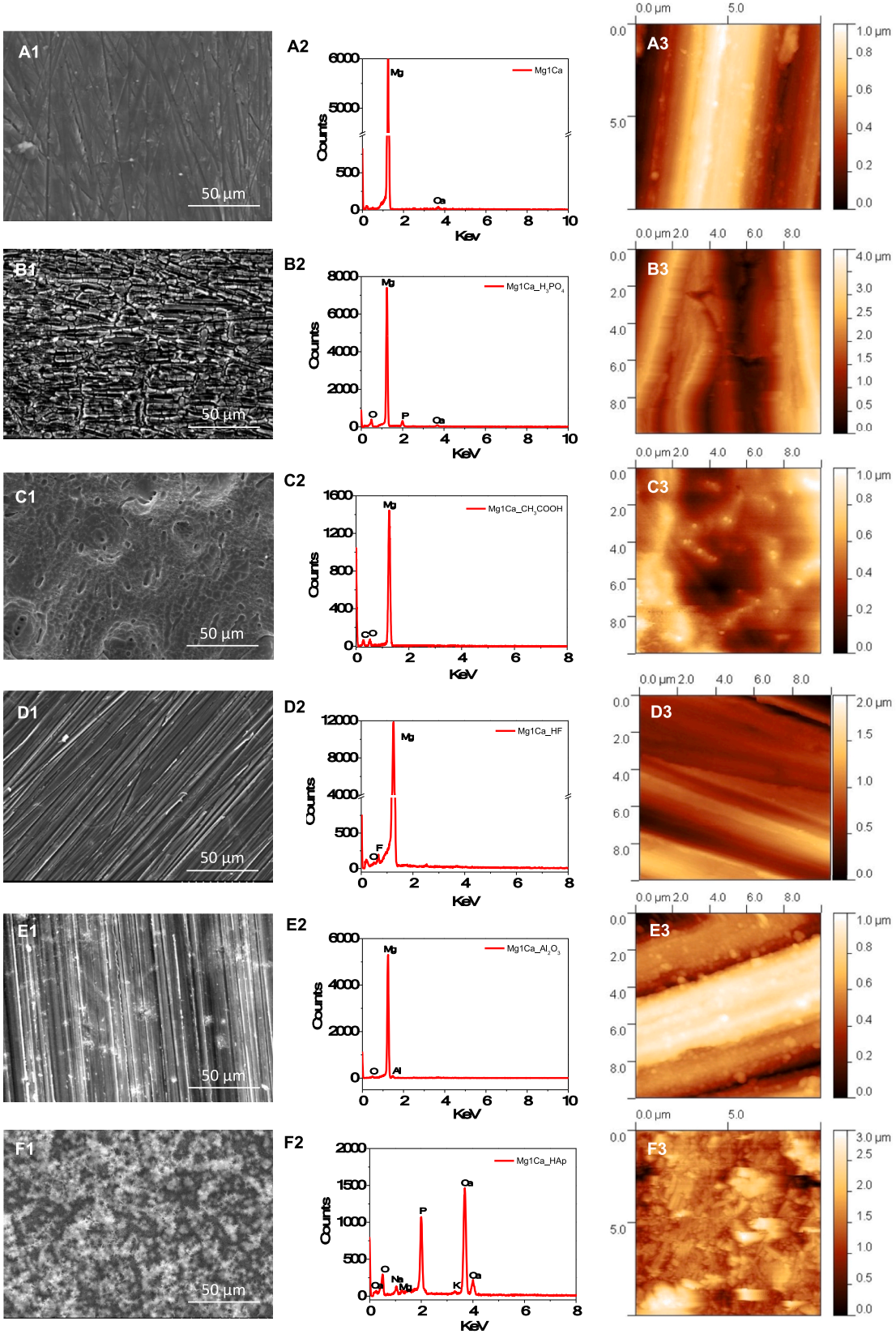

Fig. 3. SEM micrographs (A1-F1) with corresponding EDS spectra (A2-F2) and AFM topographic images (A3-F3) of (A) untreated Mg1Ca alloy and Mg1Ca substrates after surface treatments: (B) Mg1Ca-H_3PO_4; (C) Mg1Ca-CH_3COOH; (D) Mg1Ca-HF; (E) Mg1Ca-Al_2O_3; (F) Mg1Ca-HAp. SEM images were captured with a magnification of 600×, while AFM images covered an area of 10 µm × 10 µm.

Table 2
Root mean square (RMS) roughness values extracted from the AFM topographic images.

Sample	RMS Roughness (nm)
Mg1Ca	234
Mg1Ca-H_3PO_4	736
Mg1Ca-HAp	409
Mg1Ca-HF	253
Mg1Ca-Al_2O_3	224
Mg1Ca-CH_3COOH	181

contributes to this amorphous nature, as short exposure times can hinder the development of well-ordered crystalline structures. Additionally, no peaks related to the possible formation of MgF_2, $Mg(OH)xF_{2-x}$ or $Mg(CH_3COO)_2$ phases were observed, likely due to the low film thickness, as suggested by SEM, EDS, and GDOES analysis. These reduced thicknesses likely weaken the signal intensity, explaining the absence of detectable crystalline phases in the XRD results.

3.3. Chemical analysis and surface elemental profiles

Chemical analysis and surface elemental profiling of the surface-treated Mg1Ca substrates were conducted using GDOES (Fig. 5). From GDOES depth profiles, three main regions can be observed on Mg1Ca alloy samples after pre-treatments. Region I corresponds to the layer formed during the surface treatment step, region II is ascribed to the transition from the outer (film) to the inner (alloy) layer and region III to the substrate.

Fig. 5A represents the depth profile of the bare substrate where only Ca and Mg profiles are observed, which allows to identify the substrate region on GDOES depth profile of the surface treated samples. In Fig. 5B, depth profile of Mg1Ca-H_3PO_4 sample, region I ($0 < t < 10$ s) corresponds to a thin layer rich in P and with the presence of O and Ca, consistent with the existence of a film of calcium phosphate. Region II ($10\text{ s} < t < 40$ s) is considered as a transition region from the outer layer to the alloy, where it can be observed the decrease of P and O signals from the film layer and the increase of the Mg and Ca signals from the substrate. The peak in the Ca signal in this transition region, is consistent with the enrichment of Ca in the alloy. Region III ($t > 40$ s) is ascribed to the substrate, where the most intense signals correspond to Mg and Ca, the major constituents of the alloy under study (Mg1Ca).

In the case of the Mg1Ca-HF treated sample, and contrary to what was observed in the EDS spectrum (Fig. 3-D3), GDOES depth profile (Fig. 5C) does not present any peak related with fluorine. This element could not be measured due to the use of an argon plasma, which has low efficiency for excitation of optical emission from fluorine [55]. The Mg and O profiles in the very beginning of the measurement ($0 < t < 5$ s – region I) supports the previously suggested formation of a thin Mg $(OH)_xF_{2-x}$ surface layer based on the EDS results. Moreover, the Mg and Ca signals rise relatively steeply during sputtering time until reaching the substrate characterized by the plateau approximately at $t = 90$ s (region III), suggesting once more that the formed film is thin. In Fig. 5 D the GDOES depth profile of the Mg1Ca-CH_3COOH sample is presented. In region I ($0 < t < 5$ s) a signal arising from C can be observed, that may be related with the presence of a thin layer of a magnesium acetate [25]. Though, one can look at Mg and Ca profiles to have an idea of the thickness of the formed film. These profiles start to become more intense just in the beginning of the measurement ($t > 5$ s) which corresponds to the transition region, reaching the alloy at $t = 30$ s (region III) indicating that if there is any film deposited on the substrate, it is thin, as previously suggested by SEM and EDS analyses.

Regarding the atomic layer deposition of alumina (Fig. 5E) we can observe that there is a full layer of Al and O consistent with the deposition of an Al_2O_3 film (region I). This Al_2O_3 layer is somehow similar in thickness when compared to the calcium phosphate one, since it takes similar time to reach the substrate region. In Fig. 5F the depth profile of Mg1Ca-HAp suggests the presence of a thicker outer layer (region I) mostly composed by Ca and P consistent with the formation of the hydroxyapatite film.

Comparing the depth profiles of the Mg1Ca alloys subject to the different surface treatments, the main difference observed is the thickness of the film formed onto the substrates surface, being the sample treated with hydroxyapatite the one with a thicker film deposited, which can be observed by the longer time that it takes to reach region III ascribed to the substrate.

In summary, GDOES analysis is in good agreement with the results obtained by SEM/EDS, showing that after the different treatments, the films formed on the surface of the Mg substrates are very thin. By considering similar sputtering rates and sample densities, GDOES facilitates a comparative analysis of film thickness among all the applied surface treatments. Interestingly, the results indicate that HAp allows for the formation of the thickest film among all the treatments.

Moreover, SEM analysis of cross-sections (images provided in the supporting information, _Fig. S1) further corroborates these findings. Determination of film thickness is challenging. However, based in the difference on conduction contrast between the coating and the substrate, the films thickness were found to be around 19 and 34 nm, with the thickness for HAp being the highest (approximately 34 nm). These

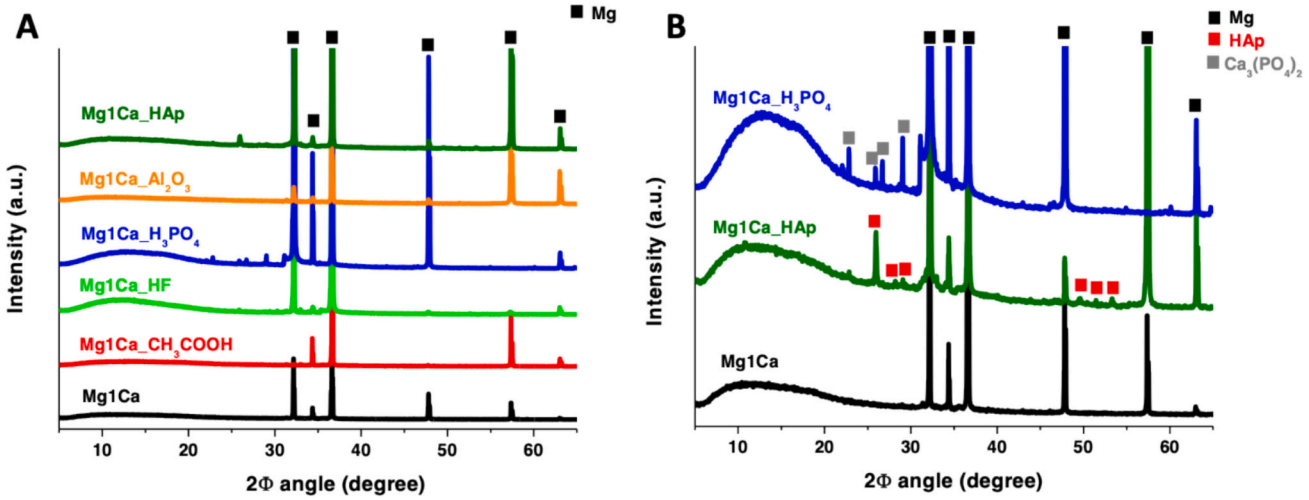

Fig. 4. X-ray diffraction (XRD) patterns of: (A) Mg1Ca alloy before and after different pre-treatments; (B) Mg1Ca, Mg1Ca-H_3PO_4 and Mg1Ca-HAp samples with identification of the crystal phases present.

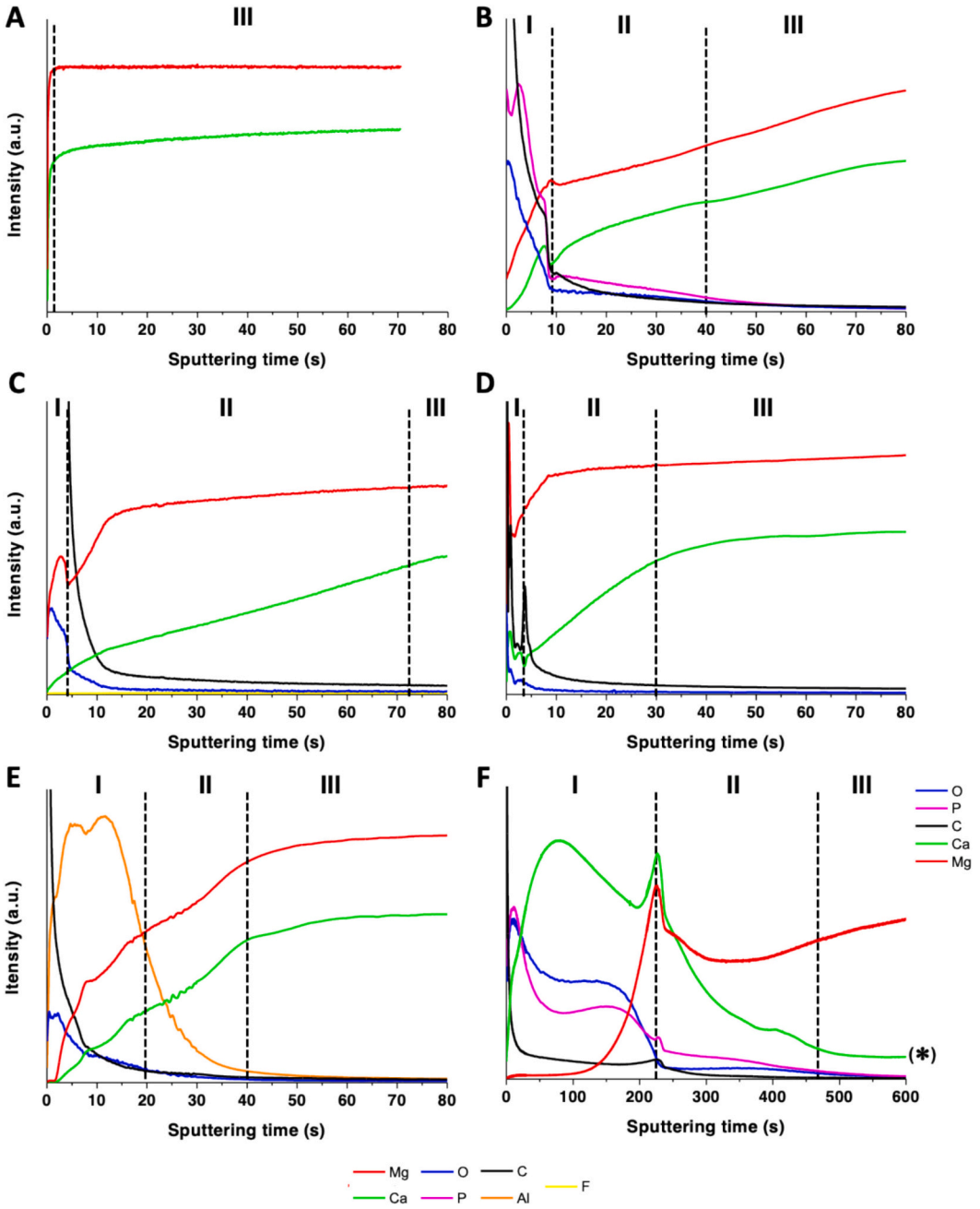

Fig. 5. Qualitative GDOES depth profiles of Mg1Ca substrates before and after pre-treatments: A – Bare substrate; B – Mg1Ca-H_3PO_4; C – Mg1Ca-HF; D – Mg1Ca-CH_3COOH; E – Mg1Ca-Al_2O_3; F – Mg1Ca-HAp. (*) in the sample Mg1Ca-HAp, Ca signal was divided by 10 due to its very high intensity, thus avoiding to obtain the signal of the others elements on background level.

values are in agreement with the GDOES results, reinforcing the conclusion that HAp treatment leads to the thickest film deposition on the Mg1Ca alloy substrates.

From the results presented so far it is possible to confirm that the different surface treatments influence surface topography and roughness properties, mostly producing thin films. Furthermore, with the exception of HAp and H_3PO_4 surface treatments, which seem to present some additional crystalline phases alongside the amorphous material, the other films are essentially amorphous.

3.4. Electrochemical impedance spectroscopy

3.4.1. Mg1Ca in MEM

The corrosion behavior of Mg1Ca in MEM, has already been studied in a previous work [3]. Fig. 6A depicts the EIS spectra for bare Mg1Ca in MEM during a 48 h immersion period in MEM. The qualitative analysis of EIS data demonstrate that the impedance magnitude increases with the immersion time, as a result of the buildup of a protective layer which drastically reduces the corrosion of the alloy [3]. In direct contact with MEM, Mg1Ca may find all the ingredients to keep a fairly stable corrosion products layer namely carbonates, phosphates, magnesium and calcium ions, as well as a suitable pH range.

However, when considering the attempt to modify Mg1Ca with a protective organic coating to induce further decrease in corrosion degradation, the results obtained are the opposite. Previous attempts by our research group, revealed that the adhesion of biodegradable polymeric coatings to Mg tends to be hampered by the reactivity of Mg in the presence of H_2O. As an example, Fig. 6B and C shows optical

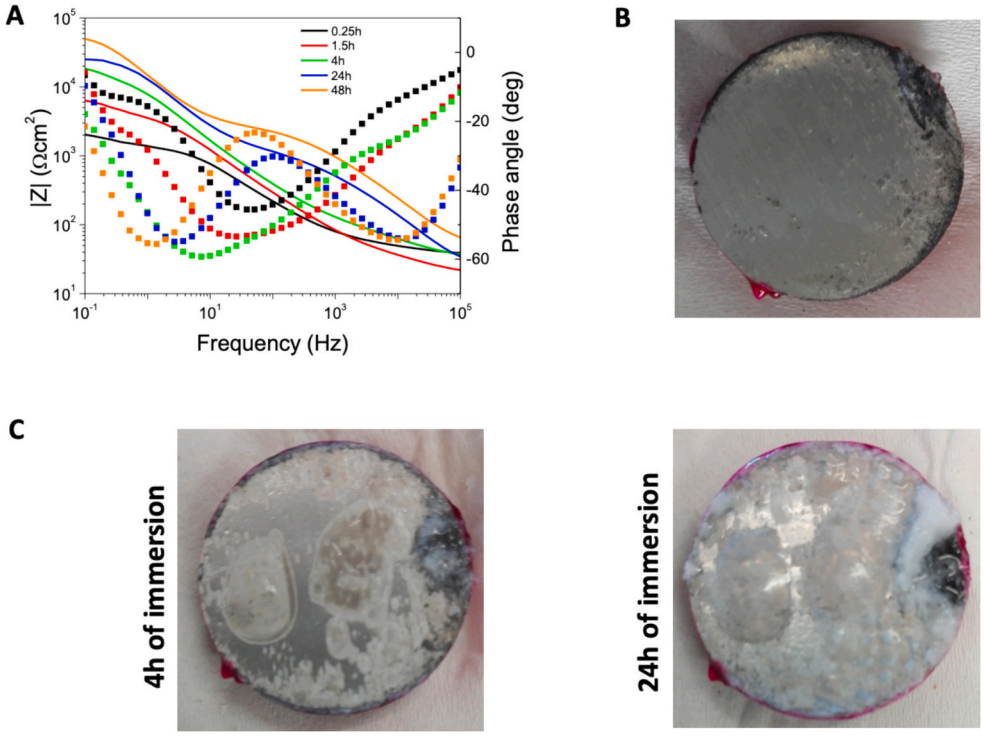

Fig. 6. (A) Bode representation of EIS spectra acquired for bare Mg1Ca in MEM, from 0.25 h to 48 h of immersion (full line corresponds to |Z| and dotted line corresponds to phase angle) – adapted from [3]; (B) Mg1Ca coated with an organic layer of PEI; (C) Mg1Ca coated with PEI after 4 h and 24 h immersion in MEM.

photographs of Mg1Ca coated with polyetherimide (PEI), before and after immersion in MEM. After immersion up to 24 h it is possible to observe signs of corrosion, with formation of blisters and subsequent coating detachment (Fig. 6C), most probably due to hydrogen evolution and cathodic delamination. Therefore, these results unambiguously show that before application of the protective organic coating layer, it is necessary to stabilize the Mg1Ca surface. In the present study, surface stabilization was achieved through specific surface treatments, and our evaluation of coating adhesion was primarily based on visual inspections following both corrosion and cytotoxicity tests. These inspections did not reveal any noticeable detachment or flaking of the coatings from the surfaces, suggesting strong adhesion under the specific conditions employed in our study (immersion in minimum essential medium – MEM). (see supporting information, -Figs. S2 and S3).

3.4.2. Mg1Ca surface-treated samples

All treated samples were analyzed by EIS to assess their corrosion protective properties and to determine what surface treatments can prevent or delay the corrosion processes of the Mg alloy under study. Those results are shown as Bode plots in Fig. 7A-E for 15 min and 24 h immersion in MEM solution. Fig. 7F presents the overlapping of impedance magnitude for Mg1Ca substrates with different treatments, after 24 h of immersion in MEM, for the sake of comparison.

The qualitative analysis of the EIS spectra shows different trends depending on the surface treatment. While in the case of the Mg1Ca-H_3PO_4 and Mg1Ca-CH_3COOH treated samples, as well as after the growth of the HAp layer (Mg1Ca-HAp), the magnitude of the impedance at low frequency increases in MEM as a function of immersion time (15 min to 24 h), the impedance magnitude associated with the Mg1Ca-Al_2O_3 and Mg1Ca-HF samples decreases. In the case of the Mg1Ca-H_3PO_4, Mg1Ca-CH_3COOH and Mg1Ca-HAp it seems that there is a positive effect of MEM components in building up of protective properties of the conversion films. This can be visualized by the increase of the phase angle at high frequency with increase of immersion time, as well as the increase of impedance magnitude at low frequency with time, that is correlated to the corrosion rate. Moreover, the decrease in |Z| after treatment with HF is very significant, with the impedance after 24 h being very low. The not so high stability of the alumina layer deposited by ALD as a function of time may be due to the lower stability of a defective Al_2O_3 layer in chloride-containing solutions (thin and amorphous-like layer) [43]. When comparing the EIS spectra acquired in MEM after 24 h, the best performing system is Mg1Ca-HAp.

Looking more specifically into the behavior of the best surface treatment among those studied in this work, namely Mg1Ca-HAp (Table 3), it is possible to see that EIS spectra have two well defined relaxation processes for short (0.25 h) as well as longer (24 h) time of immersion. The higher frequency time constant can be assigned to the conversion layer, which may grow during the immersion in MEM. The low frequency response is associated to the barrier MgO film present at the metal interface. The asymmetry in phase angle or a strongly degraded time constant at low frequencies represents the corrosion process, which inherently has characteristics close to non-polarisable electrode. For lower frequencies a third time constant may occur, but it is not possible to fit the EIS data in this frequency region due to the scattering of data. The EIS data were fitted using the equivalent circuit presented in Fig. 7G.

As the time of immersion progresses, there seems to occur a buildup in the protective layer in the case of surface treatments except alumina and HF systems. This is not totally unexpected as the ingredients that can offer protective ability to Mg1Ca directly in MEM, which coincide also with chemical composition of HAp (Ca, Mg, phosphates, hydroxides), are available in solution and in the substrate [3,56].

The effectiveness of corrosion protection provided by coatings can be significantly influenced by factors such as microstructure, chemical composition, and coating thickness. While several studies indicate that an increase in surface roughness typically results in reduced corrosion resistance in Mg alloys [57–60] our findings suggest that this trend is not universally applicable. Pre-treatments such as, H_3PO_4 and HAp, showed improved corrosion resistance despite increasing surface roughness. This implies that factors such as the chemical composition of the

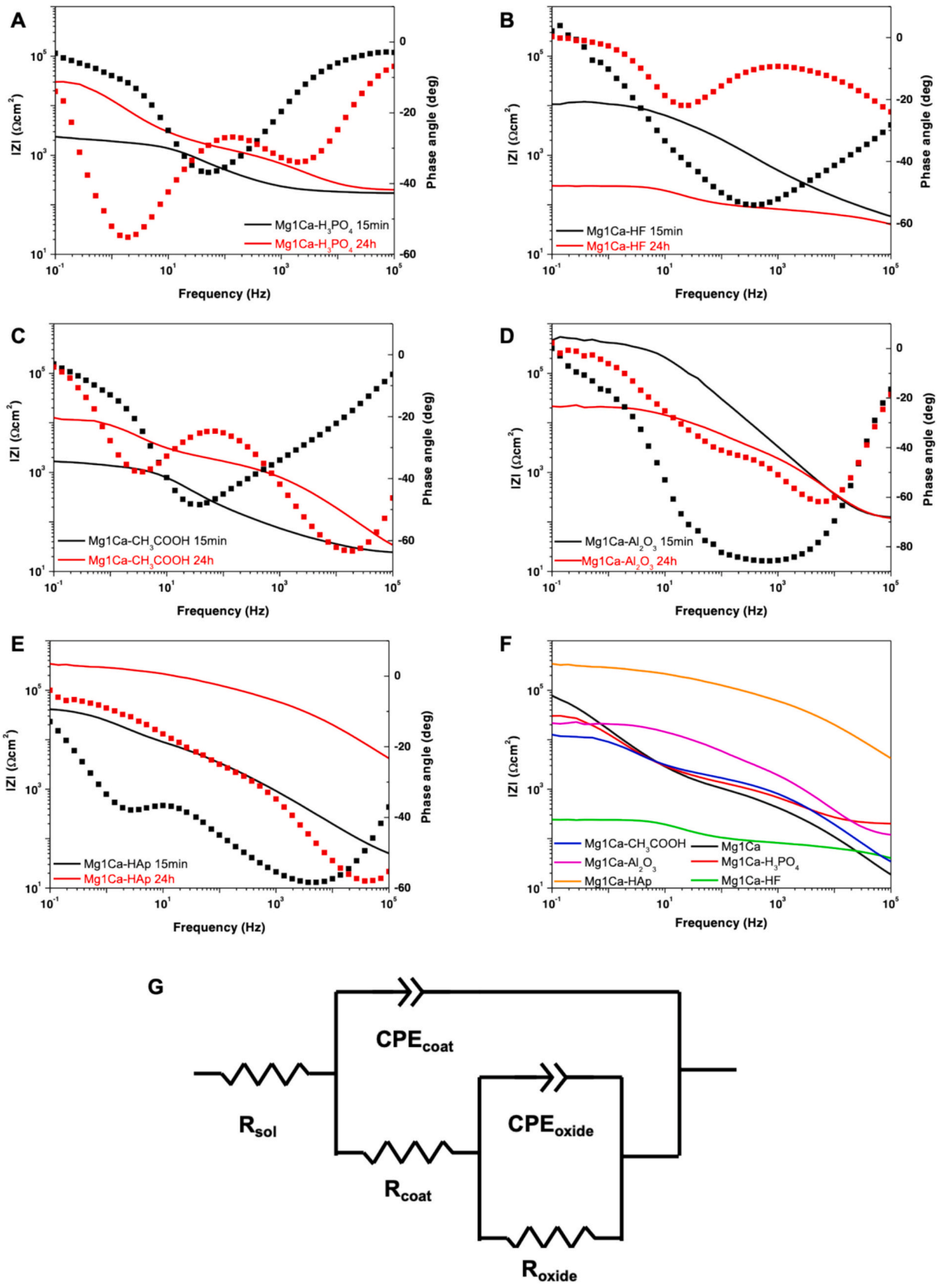

Fig. 7. (A-E): Bode representation of EIS spectra acquired for Mg1Ca with different surface treatments in MEM, after 15 min and 24 h of immersion (full line corresponds to |Z| and dotted line corresponds to phase angle); (F): Comparison of impedance magnitude after 24 h of immersion; (G): EC circuit used to fit EIS impedance for Mg1Ca-HAp system (Constant-phase elements were used instead of pure capacitors).

Table 3
Fittings for Mg1Ca-HAp surface treatment.

t/h	R_{sol} Ω cm^2	R_{coat} Ω cm^2	CPE_{coat} Ss^ncm^{-2}	n_{coat}	R_{oxide} Ω cm^2	CPE_{oxide} Ss^ncm^{-2}	n_{oxide}	X^2
0.25	23 ± 1	$9.3 \pm 0.4 \times 10^3$	$6.7 \pm 0.3 \times 10^{-7}$	0.64 ± 0.4	$2.0 \pm 0.1 \times 10^4$	$2.8 \pm 0.2 \times 10^{-5}$	0.76 ± 0.4	5.2×10^{-4}
24	30 (*)	$8.3 \pm 1.2 \times 10^4$	$1.9 \pm 0.3 \times 10^{-8}$	0.70 ± 0.01	$2.5 \pm 0.3 \times 10^5$	$4.2 \pm 1.01 \times 10^{-7}$	0.50 ± 0.05	3.6×10^{-4}

(*) parameter was fixed as there was high uncertainty in the fitting of this parameter.

coatings/films formed during these pre-treatments could have a more dominant influence on corrosion behavior.

The key observation is that depending on the surface treatments applied, the evolution of the Mg alloy system in MEM differs significantly. In the cases of phosphate and acetate-based conversion layers, an improvement of the corrosion resistance can be observed as a result of precipitation of the dense protective layer constituted by the components of MEM and Mg alloy. In contrast, the thin oxide or fluoride layers do not provide similar ptotection, leading to a decrease in corrosion resistance over time during immersion in MEM.

3.5. Cytotoxicity evaluation of the surface-treated Mg1Ca extracts (indirect testing)

Cells underwent a 24-h exposure to Mg1Ca extracts, followed by a cytotoxicity assessment based on two established endpoints: the release of LDH, as a marker of the integrity of the plasma membrane, and the reduction of WST-1, as indicator of the cellular metabolic activity. Extracts of the bare and surface-modified Mg1Ca alloy were prepared and tested for cytotoxicity in L929 fibroblast cells. As depicted in the Fig. 8, L929 cells exposed to the 24-h extracts of Al_2O_3-, HF- and CH_3COOH-coated Mg1Ca alloys exhibited a significant increase in LDH extracellular levels (Fig. 8A) and a decrease in WST-1 reduction (Fig. 8B) when compared to the respective controls. On the other hand, exposure to the HAp- and H_3PO_4-coated Mg1Ca extracts did not significantly affected the viability of L929 fibroblast cells. A similar trend was observed in cells exposed for 24 h to the 72-h extracts (Fig. 9). Thus, comparing the effects induced by exposure to the direct extract of bare vs surface-modified Mg1Ca alloys we found that while Al_2O_3-, HF- and CH_3COOH-coated Mg1Ca alloys induced higher cytotoxicity in L929

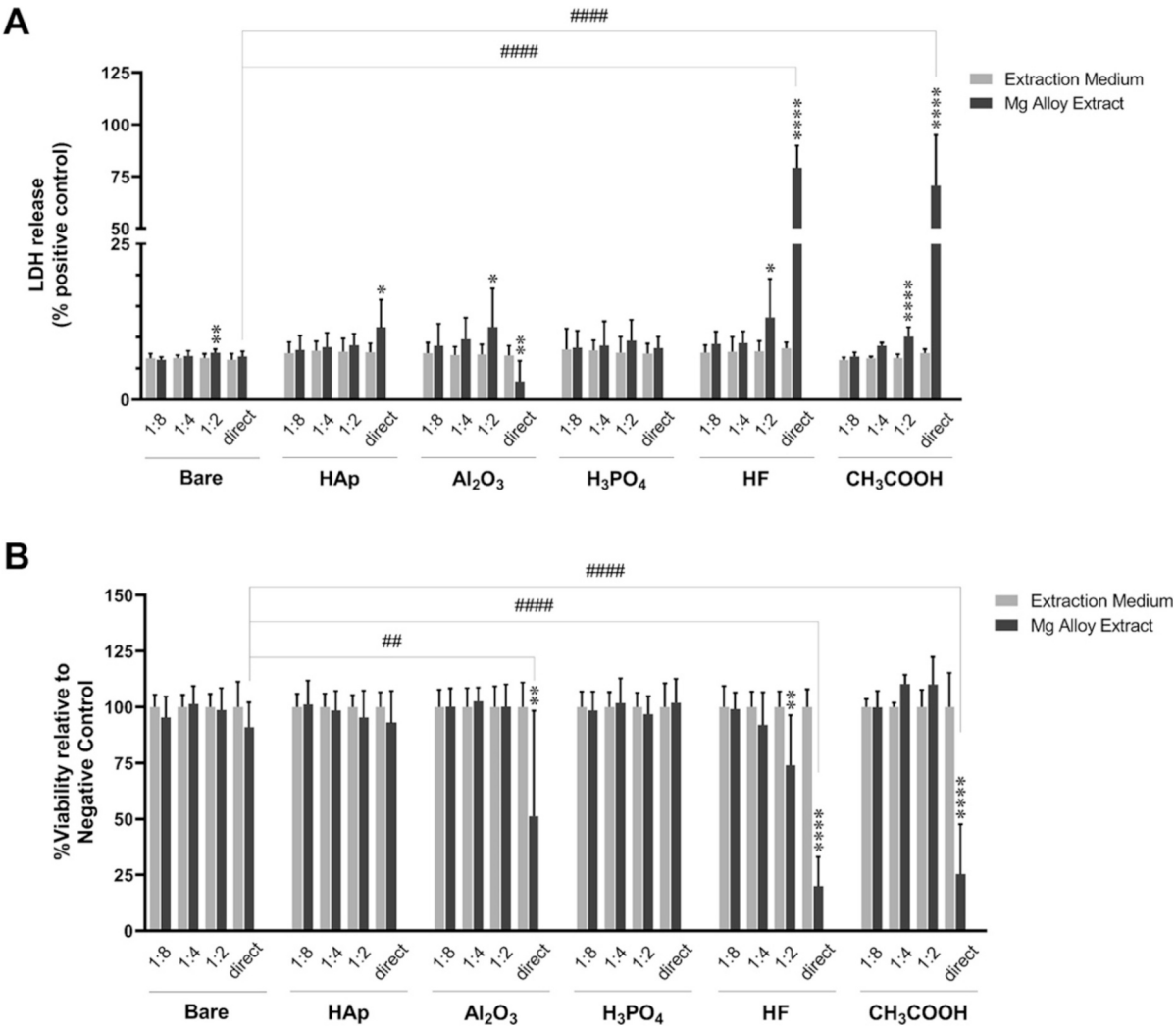

Fig. 8. Effect of extracts of the surface-stabilized Mg1Ca alloys in L929 cells viability after a 24 h exposure. (A) Plasma membrane integrity (LDH release) and (B) cell metabolic activity (WST-1 reduction) after 24 h exposure to the 24-h extracts. Data are represented by the mean ± standard deviation (SD) of 3–4 independent experiments, each performed in triplicate. Data was analyzed using the one-way ANOVA test followed by the Tukey's post hoc test to compare the direct extract of bare Mg1Ca alloy with the direct extract of the coated Mg alloy extracts (# $p < 0.05$, ## $p < 0.01$, ### $p < 0.001$; #### $p < 0.0001$ vs bare Mg1Ca).

cells, no significant differences were observed for HAp- or H_3PO_4-coated Mg1Ca.

Surface modifications not only enhance the mechanical properties and corrosion resistance of Mg alloys but also improve their biological functions, such as biocompatibility and bioactivity. [57] Reports in the literature, on the effect of Mg corrosion on cell viability are ambivalent as there are reports that indicate survival of cells while others report cell death, mainly due to the different types of alloys and cell lines used according to Lorenz et al. [60]

The work by Keim et al. [61] demonstrated that simple chemical surface treatments, such as the formation of a biomimetic layer of Ca, P, and C, could control the corrosion rate of pure Mg, reducing Mg ion release and promoting cell adhesion. The HAp layer in our study, which consists of Ca and P, provides similar benefits by enhancing corrosion resistance while maintaining biological compatibility. In our cytotoxicity evaluations, Al_2O_3-, HF-, and CH_3COOH-coated Mg1Ca alloys exhibited increased cytotoxicity, likely due to higher Mg ion release, while HAp- and H_3PO_4-coated alloys showed no significant negative impact on cell viability. The formation of a HAp layer, which mimics natural bone composition, not only enhances corrosion resistance but also maintains favorable biological interactions, aligning with previous studies [61]. These findings highligth the importance of surface modification in balancing degradation rate and biocompatibility in Mg alloys, making HAp and H_3PO_4 pre-treatments particularly promising for biomedical applications.

3.6. Role of crystallinity in corrosion resistance and cytotoxicity

The crystalline structure of materials used in protective coatings plays a critical role in influencing both the corrosion resistance and cytotoxicity of Mg alloys in biomedical applications. These properties are interrelated, as the stability of amorphous versus crystalline phases affects the materials long-term behavior in biological environments, where degradation leads to ion release which impacts both corrosion performance and biological compatibility.

In the case of hydroxyapatite (HAp), its crystallinity is known to affect its biological interactions and dissolution behavior. A study by Anjos et al. [62] demonstrated that nanostructured carbonated hydroxyapatite (nCHA) exhibited comparable in vitro biocompatibility across varying crystallinities, with no cytotoxic effects. However, Chou et al. [63] demonstrated that higher crystallinity in HAp coatings resulted in reduced pH changes in culture media, thereby lowering the risk of cytotoxicity. This suggests that crystalline HAp coatings offer better protection against ion release and medium alkalization, improving both corrosion resistance and long-term implant integrity. In contrast, lower crystallinity may accelerate initial bone formation but compromises long-term stability as the structure degrades faster [64].

For alumina (Al_2O_3), its crystalline phases, particularly α-alumina, are recognized for their superior chemical stability and corrosion resistance [65]. However, studies on Al_2O_3 nanoparticles have shown that crystalline phase and particle size significantly impact cytotoxicity

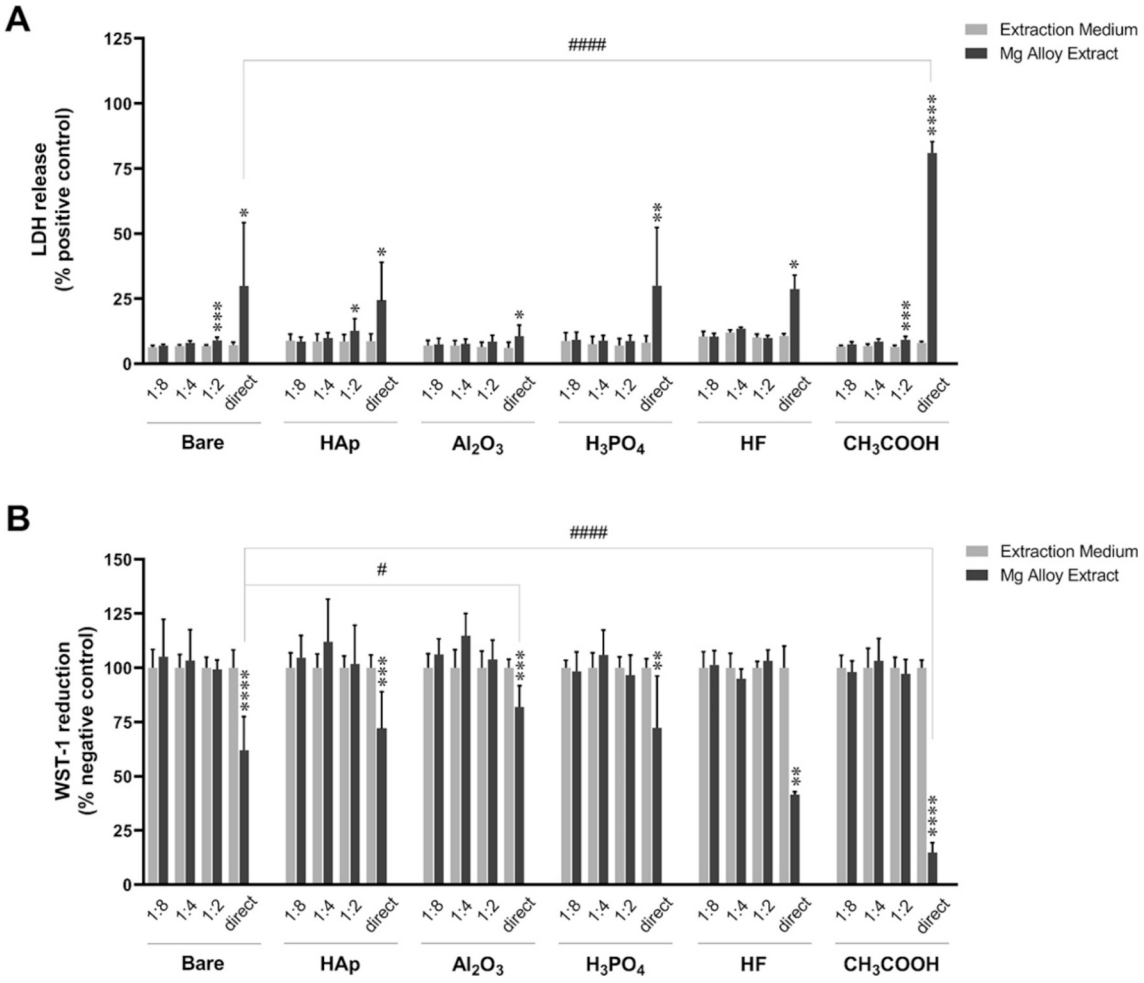

Fig. 9. Effect of extracts of the surface-stabilized Mg1Ca alloys in L929 cells viability. (A) Plasma membrane integrity (LDH release) and (B) cell metabolic activity (WST-1 reduction) after 24 h exposure to the 72-h extracts. Data are represented by the mean ± standard deviation (SD) of 3–4 independent experiments, each performed in triplicate. Data was analyzed using the one-way ANOVA test followed by the Tukey's post hoc test to compare the direct extract of bare vs surface-modified Mg1Ca alloys. # $p < 0.05$, #### $p < 0.0001$ vs bare Mg1Ca.

[66]. Exposure to γ/δ-phase Al_2O_3 nanoparticles induced DNA damagee and glutathione depletion, highlighting the cytotoxic potential of less stable phases. Amourphous Al_2O_3 coatings, particularly those grown by Atomic Layer Deposition (ALD), have shown slight cytotoxicity and limited biocompatibility, especially in long-term applications [67]. In addition to cytotoxicity, the crystallinity plays a significant role in enhancing corrosion resistance. Van Gestel et al. [68] reported that highly crystalline Al_2O_3 provides stronger corrosion protection in harsh environments compared to its less crystalline counterparts. This suggests that crystalline Al_2O_3 layers offer enhanced chemical stability and corrosion protection, crucial for long-term material stability in biomedical applications.

In our study, the crystalline hydroxyapatite (HAp) coating demonstrated superior corrosion protection by forming a stable barrier that reduced Mg1Ca degradation in MEM and minimized Mg ion release, which corresponded to reduced cytotoxicity as confirmed by our LDH and WST-1 assays. In contrast, the amorphous Al_2O_3 coating exhibited lower corrosion resistance, degrading faster and releasing more ions, resulting in increased cytotoxicity due to its poorer chemical stability, consistent with previous findings on amorphous coatings and Al_2O_3 nanoparticles [66,67].

Overall, crystallinity plays a pivotal role in both corrosion resistance and cytocompatibility. Crystalline coatings degrade more slowly, releasing fewer ions, which improves corrosion resistance and minimizes cytotoxic effects. Conversely, amorphous coatings degrade rapidly, leading to higher ion release, faster corrosion, and increased cytotoxicity. These findings underscore the importance of crystallinity in optimizing the protective and biological performance of Mg alloys in biomedical applications.

3.7. Mechanisms in the origin of corrosion protection and cytotoxic effects

Crystallinity is not the single factor influencing the effectiveness of surface treatments. Other parameters such as chemical composition, thickness, adhesion and roughness can affect the way the substrate is protected against degradation [12,58,59,69] and how it affects cellular growth and proliferation [70]. As all of these parameters were not examined separately in this study - it would also go beyond the scope of the work - the complex interplay between them cannot be fully disclosed, but their effect can only be partially assumed.

In the case of the modification with the three acids, the type of layer formed is thin and amorphous, which enables a faster dissolution of chemical layers formed, thereby enabling higher corrosion rates. Similarly, the aluminium oxide layer prepared by ALD generates a thin, amorphous layer that can dissolve/be attacked fast by chlorides, exposing Mg1Ca and enhancing its corrosion. With faster dissolution of Mg1Ca (i.e. fast kinetics and therefore high corrosion rates), the excess of Mg^{2+} can be the reason for cytotoxic effects observed for in Al_2O_3-, HF-, and CH_3COOH-coated Mg1Ca alloys. Moreover, in the case of HF and Al_2O_3, F and Al ions released can additionally contribute to the cytotoxic effects observed. The presence of these layers may also have a negative impact on the growth of the naturally developed protective layer, known to protect Mg1Ca within specific conditions, when directly exposed to MEM [3,56].

In the case of the H_3PO_4-coated Mg1Ca, the layer grown is relatively thin and offers low protection against corrosion when compared to the bare alloy as mentioned before, possibly affecting the way the naturally, amorphous-like corrosion product layer could be developed (recall Fig. 7F, especially impedance at low frequencies). However, its performance is not far from bare Mg1Ca after 24 h of immersion and its cytoxicity is also low (Figs. 8 and 9). The reason for this is that phosphates are also present in MEM and can grow as part of the protective corrosion product layer. At the same time, the low cytotoxicity observed for H_3PO_4-coated Mg1Ca, can be due to a lower dissolution of Mg^{2+}, when compared to Al_2O_3-, HF-, and CH_3COOH-coated Mg1Ca, and to the fact that phosphates are biologically relevant compounds not inducing additional detrimental effects [2,27]. Finally, the best system, HAp-coated Mg1Ca, is thicker, more crystalline than the other tested surface treatments and composed of low toxic compounds. It acts as a truly effective barrier against ingress of electrolyte, thereby preventing corrosion attack of Mg1Ca, while the relative low release of Ca and phosphates has a relative low effect on the cellular viability.

4. Conclusions

In this work, different surface treatments were applied to Mg1Ca biodegradable alloy, influencing both surface topography and roughness. Most of the treatments resulted in the formation of amorphous thin films, with the notable exception of Mg1Ca-HAp, which formed a crystalline material and exhibited the thickest protective layer among the tested treatments. EIS analysis showed that the HAp layer provided the best corrosion protection, with significantly higher impedance values compared to other treatments after 24 h immersion in MEM. Both the HAp and H_3PO_4 treatments also demonstrated promising biocompatibility, as L929 cells exposed to their extracts showed no significant cytotoxicity compared to controls. The biological relevance of HAp, coupled with its corrosion protective and non-cytotoxic characteristics, undersores its potential for further development into multilayer coatings for biomedical applications. This study paves the way for future research aimed at optimizing surface treatments to enhance the performance and safety of Mg alloys in medical devices.

CRediT authorship contribution statement

C.S. Neves: Conceptualization, Methodology, Investigation, Visualization, Formal analysis, Writing – Original draft preparation, Writing – review & editing, Funding acquisition. **I. Sousa:** Writing – review & editing, Visualization, Investigation, Funding acquisition. **M.A. Freitas:** Investigation. **L. Moreira:** Investigation, Formal analysis. **C. Costa:** Investigation. **J.P. Teixeira:** Resources. **S. Fraga:** Writing – review & editing, Visualization, Methodology, Investigation, Formal analysis. **R. M. Silva:** Investigation. **R.F. Silva:** Resources. **M. Starykevich:** Writing – review & editing, Investigation. **N. Scharnagl:** Writing – review & editing, Resources. **M.L. Zheludkevich:** Writing – review & editing. **M. G.S. Ferreira:** Writing – review & editing. **J. Tedim:** Writing – review & editing, Resources, Project administration, Funding acquisition, Conceptualization.

Funding

This work was financed by Portugal 2020 through European Regional Development Fund (ERDF) in the frame of Operational Competitiveness and Internationalization Programme (POCI), in the scope of the project MAGICOAT POCI-01-0145-FEDER-016597/PTDC/CTM-BIO/2170/2014 and in the scope of the project CICECO-Aveiro Institute of Materials, UIDB/50011/2020 (DOI 10.54499/UIBD/50011/2020), UIDP/50011/2020 (DOI 10.54499/UIDP/50011/2020) & LA/P/0006/2020 (DOI 10.54499/LA/P/0006/2020), financed by national funds through the FCT/MCTES (PIDDAC). Furthermore, thanks are due to FCT/MCTES for the financial support through national funds to EPIUnit (UIDB/04750/2020) and ITR (LA/P/0064/2020).

Declaration of competing interest

The authors declare that they have no known competing financial interests or personal relationships that could have appeared to influence the work reported in this paper.

Appendix A. Supplementary data

Supplementary data to this article can be found online at https://doi.org/10.1016/j.surfcoat.2024.131704.

Data availability

Data will be made available on request.

References

[1] N. Li, Y. Zheng, Novel magnesium alloys developed for biomedical application: A review, J. Mater. Sci. Technol. 29 (6) (2013) 489–502, https://doi.org/10.1016/j.jmst.2013.02.005.

[2] S. Shadanbaz, G.J. Dias, Calcium phosphate coatings on magnesium alloys for biomedical applications: A review, Acta Biomater. 8 (1) (2012) 20–30, https://doi.org/10.1016/j.actbio.2011.10.016.

[3] C.S. Neves, I. Sousa, M.A. Freitas, L. Moreira, C. Costa, J.P. Teixeira, S. Fraga, E. Pinto, A. Almeida, N. Scharnagl, M.L. Zheludkevich, M.G.S. Ferreira, J. Tedim, Insights into corrosion behaviour of uncoated Mg alloys for biomedical applications in different aqueous media, J. Mater. Res. Technol. 13 (2021) 1908–1922, https://doi.org/10.1016/j.jmrt.2021.05.090.

[4] M. Esmaily, J.E. Svensson, S. Fajardo, N. Birbilis, G.S. Frankel, S. Virtanen, R. Arrabal, S. Thomas, L.G. Johansson, Fundamentals and advances in magnesium alloy corrosion, Prog. Mater. Sci. 89 (2017) 92–193, https://doi.org/10.1016/j.pmatsci.2017.04.011.

[5] Hu, H., Nie, X., & Ma, Y. (2014). Corrosion and surface treatment of magnesium alloys. Em F. Czerwinski (Ed.), Magnesium Alloys—Properties in Solid and Liquid States. InTech. doi:https://doi.org/10.5772/58929.

[6] Z.-Z. Yin, W.-C. Qi, R.-C. Zeng, X.-B. Chen, C.-D. Gu, S.-K. Guan, Y.-F. Zheng, Advances in coatings on biodegradable magnesium alloys, Journal of Magnesium and Alloys 8 (1) (2020) 42–65, https://doi.org/10.1016/j.jma.2019.09.008.

[7] H. Hornberger, S. Virtanen, A.R. Boccaccini, Biomedical coatings on magnesium alloys – A review, Acta Biomater. 8 (7) (2012) 2442–2455, https://doi.org/10.1016/j.actbio.2012.04.012.

[8] P. Tian, X. Liu, Surface modification of biodegradable magnesium and its alloys for biomedical applications, Regenerative Biomaterials 2 (2) (2015) 135–151, https://doi.org/10.1093/rb/rbu013.

[9] V. Tsakiris, C. Tardei, F.M. Clicinschi, Biodegradable Mg alloys for orthopedic implants – A review, Journal of Magnesium and Alloys 9 (6) (2021) 1884–1905, https://doi.org/10.1016/j.jma.2021.06.024.

[10] Y. Wang, C.S. Lim, C.V. Lim, M.S. Yong, E.K. Teo, L.N. Moh, In vitro degradation behavior of M1A magnesium alloy in protein-containing simulated body fluid, Mater. Sci. Eng. C 31 (3) (2011) 579–587, https://doi.org/10.1016/j.msec.2010.11.017.

[11] S. Zhang, X. Zhang, C. Zhao, J. Li, Y. Song, C. Xie, H. Tao, Y. Zhang, Y. He, Y. Jiang, Research on an Mg–Zn alloy as a degradable biomaterial, Acta Biomater. 6 (2) (2010) 626–640, https://doi.org/10.1016/j.actbio.2009.06.028.

[12] M. Pogorielov, E. Husak, A. Solodivnik, S. Zhdanov, Magnesium-based biodegradable alloys: degradation, application, and alloying elements, Interventional Medicine and Applied Science 9 (1) (2017) 27–38, https://doi.org/10.1556/1646.9.2017.1.04.

[13] L.L. Rokhlin, Magnesium Alloys Containing Rare Earth Metals: Structure and Properties, Taylor & Francis, 2003.

[14] F. Witte, J. Fischer, J. Nellesen, H.-A. Crostack, V. Kaese, A. Pisch, F. Beckmann, H. Windhagen, In vitro and in vivo corrosion measurements of magnesium alloys, Biomaterials 27 (7) (2006) 1013–1018, https://doi.org/10.1016/j.biomaterials.2005.07.037.

[15] G. Song, Control of biodegradation of biocompatable magnesium alloys, Corros. Sci. 49 (4) (2007) 1696–1701, https://doi.org/10.1016/j.corsci.2007.01.001.

[16] T. Hassel, F.W. Bach, A. Golovko, C. Krause, Investigation of the mechanical properties and the corrosion behaviour of low alloyed magnesium-calcium alloys for use as absorbable biomaterial in the implant technique, in: 45th Annual Conference of Metallurgists of CIM, 2006, pp. 359–370.

[17] Z. Li, X. Gu, S. Lou, Y. Zheng, The development of binary Mg–Ca alloys for use as biodegradable materials within bone, Biomaterials 29 (10) (2008) 1329–1344, https://doi.org/10.1016/j.biomaterials.2007.12.021.

[18] L. Xu, G. Yu, E. Zhang, F. Pan, K. Yang, In vivo corrosion behavior of Mg-Mn-Zn alloy for bone implant application, J. Biomed. Mater. Res. A 83A (3) (2007) 703–711, https://doi.org/10.1002/jbm.a.31273.

[19] Y. Wan, G. Xiong, H. Luo, F. He, Y. Huang, X. Zhou, Preparation and characterization of a new biomedical magnesium–calcium alloy, Mater. Des. 29 (10) (2008) 2034–2037, https://doi.org/10.1016/j.matdes.2008.04.017.

[20] N. Sezer, Z. Evis, S.M. Kayhan, A. Tahmasebifar, M. Koç, Review of magnesium-based biomaterials and their applications, Journal of Magnesium and Alloys 6 (1) (2018) 23–43, https://doi.org/10.1016/j.jma.2018.02.003.

[21] I.J. Polmear, Grades and alloys, in: ASM Specialty Handbook on Magnesium and Magnesium Alloys, ASM International, 1999, pp. 12–25.

[22] L.M. Calado, M.J. Carmezim, M.F. Montemor, Rare earth based magnesium alloys—A review on WE series, Frontiers in Materials 8 (2022) 804906, https://doi.org/10.3389/fmats.2021.804906.

[23] J.A. Yuwono, C.D. Taylor, G.S. Frankel, N. Birbilis, S. Fajardo, Understanding the enhanced rates of hydrogen evolution on dissolving magnesium, Electrochem. Commun. 104 (2019) 106482, https://doi.org/10.1016/j.elecom.2019.106482.

[24] W. Wu, Z. Wang, S. Zang, X. Yu, H. Yang, S. Chang, Research progress on surface treatments of biodegradable Mg alloys: A review, ACS Omega 5 (2) (2020) 941–947, https://doi.org/10.1021/acsomega.9b03423.

[25] S.A. Rahim, M.A. Joseph, T, H., Tailoring biomineralization and biodegradation of Mg–Ca alloy by acetic acid pickling, Materials Research Express 7 (5) (2020) 054002, https://doi.org/10.1088/2053-1591/ab8d5f.

[26] S.A. Rahim, V. Muhammad Rabeeh, M.A. Joseph, T. Hanas, Does acid pickling of Mg-Ca alloy enhance biomineralization? Journal of Magnesium and Alloys 9 (3) (2021) 1028–1038, https://doi.org/10.1016/j.jma.2020.12.002.

[27] D.G. Tamay, S. Gokyer, J. Schmidt, A. Vladescu, P. Yilgor Huri, V. Hasirci, N. Hasirci, Corrosion Resistance and Cytocompatibility of Magnesium–Calcium Alloys Modified with Zinc- or Gallium-Doped Calcium Phosphate Coatings, ACS Appl. Mater. Interfaces 14 (1) (2022) 104–122, https://doi.org/10.1021/acsami.1c16307.

[28] N. Li, Y.D. Li, Y.B. Wang, M. Li, Y. Cheng, Y.H. Wu, Y.F. Zheng, Corrosion resistance and cytotoxicity of a MgF_2 coating on biomedical Mg-1Ca alloy via vacuum evaporation deposition method: corrosion resistance and cytotoxicity of MgF_2 coating on Mg-Ca alloy, Surf. Interface Anal. 45 (8) (2013) 1217–1222, https://doi.org/10.1002/sia.5257.

[29] Z.J. Jia, M. Li, Q. Liu, X.C. Xu, Y. Cheng, Y.F. Zheng, T.F. Xi, S.C. Wei, Micro-arc oxidization of a novel Mg–1Ca alloy in three alkaline KF electrolytes: corrosion resistance and cytotoxicity, Appl. Surf. Sci. 292 (2014) 1030–1039, https://doi.org/10.1016/j.apsusc.2013.11.038.

[30] X.N. Gu, Y.F. Zheng, Q.X. Lan, Y. Cheng, Z.X. Zhang, T.F. Xi, D.Y. Zhang, Surface modification of an Mg-1Ca alloy to slow down its biocorrosion by chitosan, Biomed. Mater. 4 (4) (2009) 044109, https://doi.org/10.1088/1748-6041/4/4/044109.

[31] P. Xiong, Z. Jia, M. Li, W. Zhou, J. Yan, Y. Wu, Y. Cheng, Y. Zheng, Biomimetic Ca, Sr/P-doped silk fibroin films on Mg-1Ca alloy with dramatic corrosion resistance and osteogenic activities, ACS Biomater Sci. Eng. 4 (9) (2018) 3163–3176, https://doi.org/10.1021/acsbiomaterials.8b00787.

[32] P. Xiong, J. Yan, P. Wang, Z. Jia, W. Zhou, W. Yuan, Y. Li, Y. Liu, Y. Cheng, D. Chen, Y. Zheng, A pH-sensitive self-healing coating for biodegradable magnesium implants, Acta Biomater. 98 (2019) 160–173, https://doi.org/10.1016/j.actbio.2019.04.045.

[33] T, D. T., Rahim, S. A., & T, H., Polyvinyl alcohol/magnesium phosphate composite coated Mg–Ca alloy for biodegradable orthopaedic implant applications, Materials Research Express 6 (11) (2019) 1165b7, https://doi.org/10.1088/2053-1591/ab4d83.

[34] M.P. Sealy, Y.B. Guo, R.C. Caslaru, J. Sharkins, D. Feldman, Fatigue performance of biodegradable magnesium–calcium alloy processed by laser shock peening for orthopedic implants, Int. J. Fatigue 82 (2016) 428–436, https://doi.org/10.1016/j.ijfatigue.2015.08.024.

[35] M. Salahshoor, Y.B. Guo, Surface modification of biodegradable magnesium-calcium implants by burnishing, Volume 2: Biomedical and Biotechnology Engineering; Nanoengineering for Medicine and Biology (2011) 609–617, https://doi.org/10.1115/IMECE2011-63730.

[36] T.S.N.S. Narayanan, I.-S. Park, M.-H. Lee, Surface modification of magnesium and its alloys for biomedical applications, in: Surface Modification of Magnesium and its Alloys for Biomedical Applications, Elsevier, 2015, pp. 29–87, https://doi.org/10.1016/B978-1-78242-077-4.00002-4.

[37] Y. Zheng, Magnesium Alloys as Degradable Biomaterials, 1.[a] ed., CRC Press, 2015 https://doi.org/10.1201/b18932.

[38] Sigma Aldrich, (sem data). Product information: Minimum Essential Medium Eagle (MEM) Alpha Modifications. https://www.sigmaaldrich.com/deepweb/assets/sigmaaldrich/product/documents/333/863/m4526for.pdf.

[39] M. Rahman, N.K. Dutta, N. Roy Choudhury, Magnesium alloys with tunable interfaces as bone implant materials, Front. Bioeng. Biotechnol. 8 (2020) 564, https://doi.org/10.3389/fbioe.2020.00564.

[40] U.C. Nwaogu, C. Blawert, N. Scharnagl, W. Dietzel, K.U. Kainer, Influence of inorganic acid pickling on the corrosion resistance of magnesium alloy AZ31 sheet, Corros. Sci. 51 (11) (2009) 2544–2556, https://doi.org/10.1016/j.corsci.2009.06.045.

[41] A. Zomorodian, M.P. Garcia, T. Moura e Silva, J.C.S. Fernandes, M.H. Fernandes, M.F. Montemor, Corrosion resistance of a composite polymeric coating applied on biodegradable AZ31 magnesium alloy, Acta Biomater. 9 (10) (2013) 8660–8670, https://doi.org/10.1016/j.actbio.2013.02.036.

[42] T.F. Conceicao, N. Scharnagl, C. Blawert, W. Dietzel, K.U. Kainer, Corrosion protection of magnesium alloy AZ31 sheets by spin coating process with poly(ether imide) [PEI], Corros. Sci. 52 (6) (2010) 2066–2079, https://doi.org/10.1016/j.corsci.2010.02.027.

[43] M.P. Oliveira, R.M. Silva, K.A. Yasakau, A. Bastos, S. Kallip, M.L. Zheludkevich, R. F. Silva, M.G.S. Ferreira, Atomic layer deposition of nanometric alumina for corrosion protection of heterogeneous metallic surfaces – the case of aeronautical grade aluminium alloy 2024-T3, Corros. Sci. 209 (2022) 110773, https://doi.org/10.1016/j.corsci.2022.110773.

[44] S. Hiromoto, Corrosion of calcium phosphate coated AZ31 magnesium alloy under a salt spray test, Mater. Trans. 53 (4) (2012) 700–706, https://doi.org/10.2320/matertrans.M2011346.

[45] ISO 10993-12:2021 Biological evaluation of medical devices—Part 12: Sample preparation and reference materials, 2021.

[46] ISO 10993-5:2009 Biological evaluation of medical devices—Part 5: Tests for in vitro cytotoxicity. (sem data).

[47] T.F. da Conceicao, N. Scharnagl, C. Blawert, W. Dietzel, K.U. Kainer, Surface modification of magnesium alloy AZ31 by hydrofluoric acid treatment and its effect on the corrosion behaviour, Thin Solid Films 518 (18) (2010) 5209–5218, https://doi.org/10.1016/j.tsf.2010.04.114.

[48] H.R. Bakhsheshi-Rad, M.H. Idris, M.R.A. Kadir, M. Daroonparvar, Effect of fluoride treatment on corrosion behavior of Mg–Ca binary alloy for implant application,

Trans. Nonferrous Met. Soc. Chin. 23 (3) (2013) 699–710, https://doi.org/10.1016/S1003-6326(13)62519-4.
[49] T.F. da Conceição, N. Scharnagl, Fluoride conversion coatings for magnesium and its alloys for the biological environment, in: Surface Modification of Magnesium and its Alloys for Biomedical Applications, Elsevier, 2015, pp. 3–21, https://doi.org/10.1016/B978-1-78242-078-1.00001-3.
[50] C.A. Bishop, Atomic layer deposition, in: Vacuum Deposition onto Webs, Films and Foils, Elsevier, 2011, pp. 331–336, https://doi.org/10.1016/B978-1-4377-7867-0.00019-2.
[51] L. Zhang, H.C. Jiang, C. Liu, J.W. Dong, P. Chow, Annealing of Al $_2$ O $_3$ thin films prepared by atomic layer deposition, J. Phys. D Appl. Phys. 40 (12) (2007) 3707–3713, https://doi.org/10.1088/0022-3727/40/12/025.
[52] M. Jamesh, S. Kumar, T.S.N. Sankara Narayanan, Electrodeposition of hydroxyapatite coating on magnesium for biomedical applications, J. Coat. Technol. Res. 9 (4) (2012) 495–502, https://doi.org/10.1007/s11998-011-9382-6.
[53] R.-G. Guan, I. Johnson, T. Cui, T. Zhao, Z.-Y. Zhao, X. Li, H. Liu, Electrodeposition of hydroxyapatite coating on Mg-4.0Zn-1.0Ca-0.6Zr alloy and in vitro evaluation of degradation, hemolysis, and cytotoxicity, J. Biomed. Mater. Res. A 100A (4) (2012) 999–1015, https://doi.org/10.1002/jbm.a.34042.
[54] S. Shi, S. Qian, X. Hou, J. Mu, J. He, X. Chou, Structural and optical properties of amorphous Al $_2$ O $_3$ thin film deposited by atomic layer deposition, Advances in Condensed Matter Physics 2018 (2018) 1–10, https://doi.org/10.1155/2018/7598978.
[55] K. Wagatsuma, K. Hirokawa, N. Yamashita, Detection of fluorine emission lines from Grimm-type glow-discharge plasmas—use of neon as the plasma gas, Anal. Chim. Acta 324 (2–3) (1996) 147–154, https://doi.org/10.1016/0003-2670(95)00623-0.
[56] D. Mei, S.V. Lamaka, J. Gonzalez, F. Feyerabend, R. Willumeit-Römer, M. L. Zheludkevich, The role of individual components of simulated body fluid on the corrosion behavior of commercially pure Mg, Corros. Sci. 147 (2019) 81–93, https://doi.org/10.1016/j.corsci.2018.11.011.
[57] T. Zhang, W. Wang, J. Liu, L. Wang, Y. Tang, K. Wang, A review on magnesium alloys for biomedical applications, Front. Bioeng. Biotechnol. 10 (2022) 953344, https://doi.org/10.3389/fbioe.2022.953344.
[58] R. Walter, M.B. Kannan, Influence of surface roughness on the corrosion behaviour of magnesium alloy, Materials & Design 32 (4) (2011) 2350–2354, https://doi.org/10.1016/j.matdes.2010.12.016.
[59] T.L. Nguyen, A. Blanquet, M.P. Staiger, G.J. Dias, T.B.F. Woodfield, On the role of surface roughness in the corrosion of pure magnesium *in vitro*, J. Biomed. Mater. Res. B Appl. Biomater. 100B (5) (2012) 1310–1318, https://doi.org/10.1002/jbm.b.32697.
[60] C. Lorenz, J.G. Brunner, P. Kollmannsberger, L. Jaafar, B. Fabry, S. Virtanen, Effect of surface pre-treatments on biocompatibility of magnesium, Acta Biomater. 5 (7) (2009) 2783–2789, https://doi.org/10.1016/j.actbio.2009.04.018.
[61] S. Keim, J.G. Brunner, B. Fabry, S. Virtanen, Control of magnesium corrosion and biocompatibility with biomimetic coatings, J. Biomed. Mater. Res. B Appl. Biomater. 96B (1) (2011) 84–90, https://doi.org/10.1002/jbm.b.31742.
[62] S. Dos Anjos, E. Mavropoulos, G.G. Alves, A.M. Costa, M. De Alencar Hausen, C. N. Spiegel, M.M. Longuinho, M. Mir, J.M. Granjeiro, A.M. Rossi, Impact of crystallinity and crystal size of nanostructured carbonated hydroxyapatite on pre-osteoblast in vitro biocompatibility, J. Biomed. Mater. Res. A 107 (9) (2019) 1965–1976, https://doi.org/10.1002/jbm.a.36709.
[63] L. Chou, B. Marek, W.R. Wagner, Effects of hydroxylapatite coating crystallinity on biosolubility, cell attachment efficiency and proliferation in vitro, Biomaterials 20 (10) (1999) 977–985, https://doi.org/10.1016/S0142-9612(98)00254-3.
[64] E.S. Marchenko, K.M. Dubovikov, G.A. Baigonakova, A.A. Shishelova, E. B. Topolnitskiy, A.L. Chernyshova, The influence of hydroxyapatite coatings with different structure and crystallinity on osteogenesis stimulation, Ceram. Int. 50 (15) (2024) 27317–27330, https://doi.org/10.1016/j.ceramint.2024.05.029.
[65] Z. Zhao, H. Li, Z. Zheng, L. Zheng, Y. Yan, Improved thermal shock and corrosion resistance of α-Al2O3/AlPO4 coating with PAA addition, Surf. Coat. Technol. 414 (2021) 127115, https://doi.org/10.1016/j.surfcoat.2021.127115.
[66] A. Bourgois, D. Crouzier, F.-X. Legrand, F. Raffin, A. Boyard, M. Girleanu, A.-L. Favier, S. François, S. Dekali, Alumina nanoparticles size and crystalline phase impact on cytotoxic effect on alveolar epithelial cells after simple or HCl combined exposures, Toxicol. In Vitro 59 (2019) 135–149, https://doi.org/10.1016/j.tiv.2019.04.016.
[67] D. Osorio, J. Lopez, H. Tiznado, M.H. Farias, M.A. Hernandez-Landaverde, M. Ramirez-Cardona, J.M. Yañez-Limon, J.O. Gutierrez, J.C. Caicedo, G. Zambrano, Structure and surface morphology effect on the cytotoxicity of [Al2O3/ZnO]n/316L SS nanolaminates growth by atomic layer deposition (ALD), Crystals 10 (7) (2020) 620, https://doi.org/10.3390/cryst10070620.
[68] T. Van Gestel, Corrosion properties of alumina and titania NF membranes, J. Membr. Sci. 214 (1) (2003) 21–29, https://doi.org/10.1016/S0376-7388(02)00517-3.
[69] T. Wu, K. Zhang, Corrosion and protection of magnesium alloys: recent advances and future perspectives, Coatings 13 (9) (2023) 1533, https://doi.org/10.3390/coatings13091533.
[70] J. Chen, J. Dai, J. Qian, W. Li, R. Li, D. Pang, G. Wan, P. Li, S. Xu, Influence of surface roughness on biodegradability and cytocompatibility of high-purity magnesium, Materials 15 (11) (2022) 3991, https://doi.org/10.3390/ma15113991.